Molecular Cancer Therapeutics

Irreversible Inhibition of EGFR: Modeling the Combined Pharmacokinetic–Pharmacodynamic Relationship of Osimertinib and Its Active Metabolite AZ5104

James W.T. Yates[1], Susan Ashton[2], Darren Cross[2], Martine J. Mellor[2], Steve J. Powell[2], and Peter Ballard[1]

Abstract

Osimertinib (AZD9291) is a potent, selective, irreversible inhibitor of EGFR-sensitizing (exon 19 and L858R) and T790M-resistant mutation. *In vivo*, in the mouse, it is metabolized to an active des-methyl metabolite, AZ5104. To understand the therapeutic potential in patients, this study aimed to assess the relationship between osimertinib pharmacokinetics, the pharmacokinetics of the active metabolite, the pharmacodynamics of phosphorylated EGFR reduction, and efficacy in mouse xenograft models of EGFR-driven cancers, including two NSCLC lines. Osimertinib was dosed in xenografted models of EGFR-driven cancers. In one set of experiments, changes in phosphorylated EGFR were measured to confirm target engagement. In a second set of efficacy studies, the resulting changes in tumor volume over time after repeat dosing of osimertinib were observed. To account for the contributions of both molecules, a mathematical modeling approach was taken to integrate the resulting datasets. The model was able to describe the pharmacokinetics, pharmacodynamics, and efficacy in A431, PC9, and NCI-H1975 xenografts, with the differences in sensitivity described by the varying potency against wild-type, sensitizing, and T790M-mutant EGFR and the phosphorylated EGFR reduction required to reduce tumor volume. It was inferred that recovery of pEGFR is slower after chronic dosing due to reduced resynthesis. It was predicted and further demonstrated that although inhibition is irreversible, the resynthesis of EGFR is such that infrequent intermittent dosing is not as efficacious as once daily dosing. *Mol Cancer Ther; 15(10); 2378–87. ©2016 AACR.*

Introduction

Mathematical modeling has demonstrated considerable value in the design and interpretation of clinical trials (1). There has been less published in the preclinical arena; however, good examples do exist (2, 3). Very few of these preclinical modeling reports consider modeling pharmacokinetic/pharmacodynamic (PK/PD) efficacy relationships of anticancer agents across cell lines. Furthermore, there are no examples of modeling the PK/PD of targeted anticancer agents where there is a significant active metabolite. We will demonstrate here such an example. Specifically, this article will demonstrate how application of PK/PD/systems pharmacology principles are used not only to understand the linkage between drug concentration and target engagement, but also deconvolute how reduced target expression after repeat dosing of an irreversible inhibitor results in changes in tumor growth. The relative contribution of the active metabolite with a different selectivity for different mutant receptor types is also investigated. We also demonstrate how mathematical modeling can generate hypotheses about the differences observed in efficacy on short- and long-term repeat dosing of an irreversible EGFR inhibitor as well as the potential for intermittent dosing.

Osimertinib (4, 5) is an orally available, potent, irreversible inhibitor of EGFR-sensitizing (EGFRm) and T790M-resistant mutations with a margin to WT-EGFR preclinically that demonstrates profound and sustained tumor regressions in *in vivo* xenograft and transgenic disease models. In mouse plasma *in vivo*, an active desmethyl metabolite (AZ5104) has been observed. AZ5104 retains the irreversible binding Michael acceptor of osimertinib. Although AZ5104 has a similar overall pharmacologic profile to osimertinib, preclinical studies indicate that it is more potent than osimertinib against EGFR-mutant cell lines with a lower margin to EGFR wild-type activity. The structures of osimertinib and AZ5104 are shown as compounds 8 and 27 in ref. 4. The *in vitro* potency in PC9 (sensitizing mutation), NCI-H1975 (T790M mutation), and LoVo (wild type) cell lines are shown in Table 1. Note that for *in vivo* studies, the A431 xenograft was used as a model of EGFR wild-type activity due to the dependence of this model for wild-type EGFR through its high level of EGFR expression.

Quite often, the pharmacokinetics of a small molecule can be different in humans to that observed in the mouse: Specifically, drugs often have a longer half-life in man. With an active metabolite, the issue of whether the same proportion of dose

[1]Oncology DMPK, AstraZeneca, Cambridge and Alderley Park, Macclesfield, United Kingdom. [2]Oncology Biosciences, AstraZeneca, Cambridge and Alderley Park, Macclesfield, United Kingdom.

Note: Supplementary data for this article are available at Molecular Cancer Therapeutics Online (http://mct.aacrjournals.org/).

Corresponding Author: James W.T. Yates, AstraZeneca, Li Ka Shing Centre, Robinson Way, Cambridge CB20RE, United Kingdom. Phone: 44 1223 769 738; Fax: 44 1625 230 848; E-mail: James.Yates@astrazeneca.com

doi: 10.1158/1535-7163.MCT-16-0142

Table 1. Key model parameter estimates and *in vitro* data used for model construction

Parameter	Interpretation	Units	Value	95% CI
***In vitro*–derived parameters**				
Osimertinib PC9 IC_{50}	Apparent *in vitro* potency against pEGFR in Ex19del cell line	nmol/L	17	13–22
AZ5104 PC9 IC_{50}	Apparent *in vitro* potency against pEGFR in Ex19del cell line	nmol/L	2	2–3
Osimertinib NCI-H1975 IC_{50}	Apparent *in vitro* potency against pEGFR in T790M cell line	nmol/L	15	10–20
AZ5104 NCI-H1975 IC_{50}	Apparent *in vitro* potency against pEGFR in T790M cell line	nmol/L	2	2–4
Osimertinib A431 IC_{50}	Apparent *in vitro* potency against pEGFR in wild-type cell line	nmol/L	2376, 1193	NA
AZ5104 A431 IC_{50}	Apparent *in vitro* potency against pEGFR in wild-type cell line		Not tested	NA
Osimertinib LoVo IC_{50}	Apparent *in vitro* potency against pEGFR in wild-type cell line	nmol/L	480	320–720
AZ5104 LoVo IC_{50}	Apparent *in vitro* potency against pEGFR in wild-type cell line	nmol/L	33	24–45
PD and efficacy parameters				
Krec_A431	Turnover rate of phEGFR	hr^{-1}	0.06	0.015–0.0741
Kbind_A431	Maximum binding rate of drug to EGFR	hr^{-1}	1.07	0.820–1.37
Cpu50_A431	Free potency of parent	μmol/L	0.412	0.203–0.811
mPot_A431	Relative potency of metabolite	—	14.33	Fixed
Emax_A431	Maximum death rate from phEGFR inhibition	hr^{-1}	0.225	0.104–0.420
N_A431	Power term on f_{kill}	—	10	4.04–188
Krec_PC9	Turnover rate of phEGFR	hr^{-1}	0.02508	0.0161–0.0701
Kbind_PC9	Maximum binding rate of drug to EGFR	hr^{-1}	0.953	0.671–1.34
Cpu50_PC9	Free potency of parent	μmol/L	0.03437	0.0132–0.0793
mPot_PC9	Relative potency of metabolite	—	5.833	Fixed
Emax_PC9	Maximum death rate from phEGFR inhibition	hr^{-1}	0.18	0.0598–0.569
N_PC9	Power term on f_{kill}	—	211	37.4–353
Krec_NCI-H1975	Turnover rate of phEGFR	hr^{-1}	0.01809	0.00627–0.0417
Kbind_NCI-H1975	Maximum binding rate of drug to EGFR	hr^{-1}	1.17	0.87–1.35
Cpu50_NCI-H1975	Free potency of parent	μmol/L	0.0106	0.00244–0.0311
mPot_NCI-H1975	Relative potency of metabolite	—	5	Fixed
Emax_NCI-H1975	Maximum death rate from phEGFR inhibition	hr^{-1}	0.15	0.0913–0.736
N_NCI-H1975	Power term on f_{kill}	—	221	56.3–359

NOTE: The 95% CIs were calculated using sampling importance resampling.
Abbreviation: CI, confidence interval.

will be converted to the metabolite needs to be a consideration as well. This raises the issue that the pharmacology observed in animal models will not translate to the clinic due to such pharmacokinetic differences. Significant differences in the plasma protein binding of the two molecules across species also exist (see Table 1). The challenge was to use the preclinical data available from the mouse to form a view of how the pharmacokinetic profile of osimertinib results in target engagement that describes the observed efficacy in xenograft tumor models and what the contribution of the metabolite AZ5104 is to the overall *in vivo* activity.

A mathematical modeling approach was used to bridge between the different data types and understand the contribution of both parent and metabolite to *in vivo* activity. This article will demonstrate how this was achieved and includes validation of the predictive power of the model under different dosing regimens.

Materials and Methods

Xenograft studies

All studies involving animals in the United Kingdom were conducted in accordance with the UK Home Office legislation, the Animal Scientific Procedures Act 1986, and with AstraZeneca Global Bioethics Policy. All experimental work is outlined in project license number 40/3483, which has gone through the AstraZeneca Ethical Review Process. NCI-H1975 and A431 cells for *in vivo* implant were cultured in DMEM (Invitrogen) supplemented with 10% v/v FCS (Sigma Aldrich) and 1% v/v L-glutamine (Invitrogen). PC9 cells were cultured in RPMI1640 (Invitrogen) supplemented with 10% v/v FCS, 1% v/v L-glutamine, and 10% v/v M1 supplement (Egg Technologies). All cell lines were then cultured in a humidified incubator with 7.5% CO_2 at 37°C. Cells were detached using 0.05% trypsin (Invitrogen) and resuspended for implant in serum-free media. Cells (5×10^6) were implanted subcutaneously in a total volume of 0.1 mL per mouse for PC9 and NCI-H1975, and 1×10^7 cells implanted subcutaneously for A431. Both PC9 and A431 cells were implanted in 50% Matrigel. PC9 xenografts were established in female severe combined immune compromised (CB17 scid) mice, and NCI-H1975 and A431 were established in female athymic (nu/nu: Alpk) mice. All mice were greater than 6 weeks old at the time of cell implant. Tumor growth was monitored twice weekly by bilateral caliper measurements, tumor volume calculated, and mice randomized into vehicle or treatment groups with approximate mean start size of 0.2 to 0.4 cm^3. Randomization for animal studies is based on initial tumor volumes to ensure equal distribution across groups. A power analysis is performed, in which group sizes are calculated to enable statistically robust detection of tumor growth inhibition. Mice were dosed once daily by oral gavage for duration of the treatment period. Tumor growth inhibition from the start of treatment was assessed by comparison of the mean change in geometric tumor volume for the control and treated groups. Statistical significance was evaluated using a one-tailed Student *t* test.

For pharmacodynamic studies, mice were randomized at a mean tumor volume of approximately 0.5 to 0.8 cm^3 using the same randomization criteria as the tumor growth inhibition studies. Mice were then treated orally with either vehicle or osimertinib. Blood and tumor were taken at specific time points after dosing. Terminal blood samples were taken by cardiac puncture, centrifuged at 13,000 rpm, at 4°C for 3 to 4 minutes.

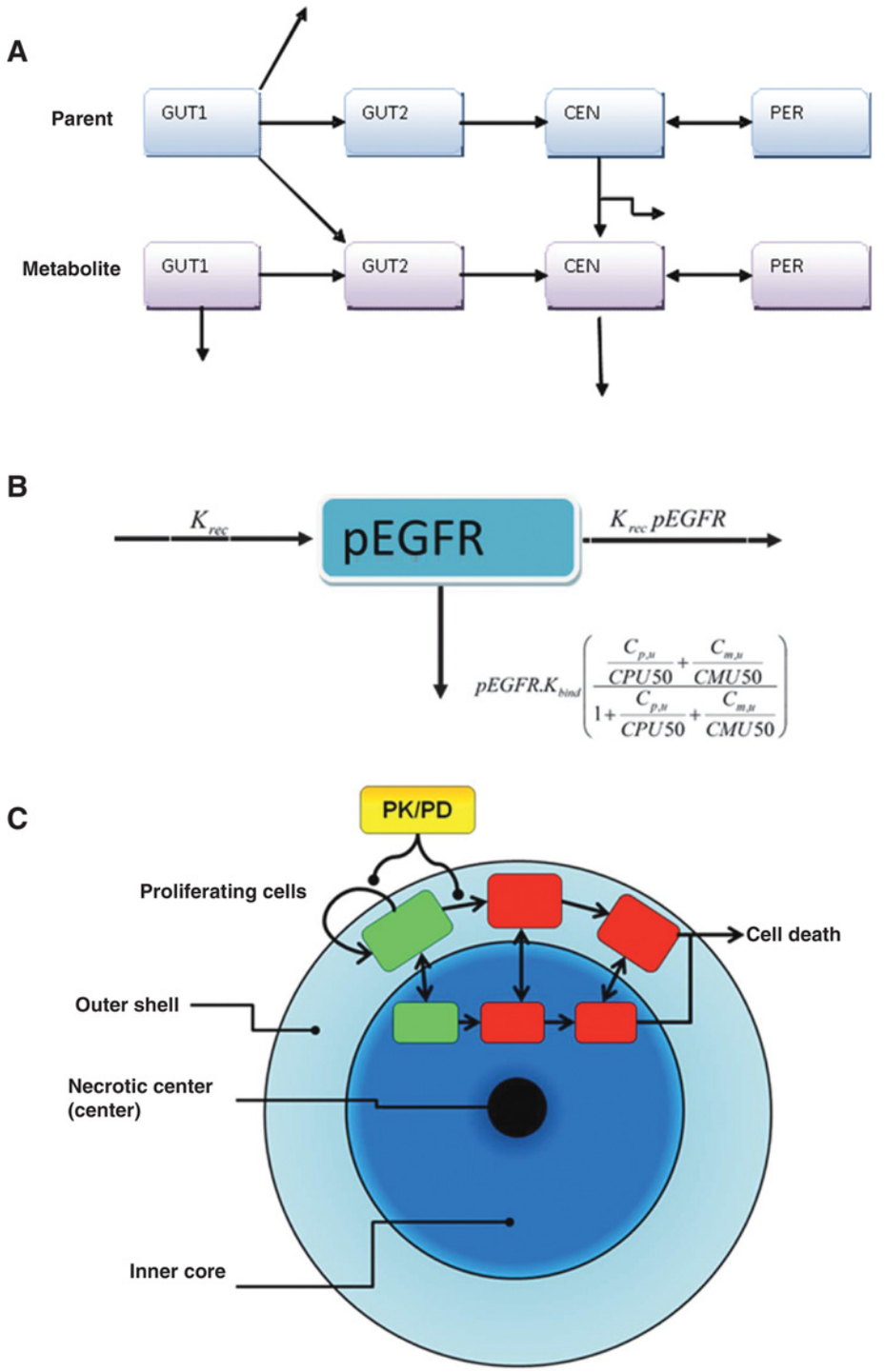

Figure 1.
Schematics of PK/PD efficacy model. **A,** parent–metabolite pharmacokinetic model. **B,** irreversible binder pharmacodynamic model. **C,** the tumor model used to describe the efficacy data observed in tumor xenografts.

Plasma was removed and stored at −80°C. Tumors were snap frozen in liquid nitrogen, followed by storage at −80°C. Tumors were homogenized by FastPrep technology in a Tris-based cell lysis buffer containing phosphatase and protease inhibitors. Detection of EGFR and phosphorylated EGFR was performed using R&D Systems ELISA Kits (DYC1854 and DYC1095, respectively). Data are expressed as percentage inhibition of phosphorylated:total protein compared with vehicle control group.

Pharmacokinetic studies

Osimertinib-free base was dissolved in dimethylacetamide (30%)/water (70%) for intravenous administration and in

polysorbate 80 (1% in water) for oral dosing to mice. The intravenous pharmacokinetics was determined in CD-1 mice at a 2 mg/kg dose and the oral pharmacokinetics in Swiss athymic nu-nu (nude) and SCID mice at doses from 1 to 25 mg/kg. Multiple micro samples were taken from each mouse. The effect of aminobenzotriazole (ABT) on the mouse pharmacokinetics of 25 mg/kg osimertinib was evaluated with a dose of ABT (50 mg/kg once daily 1 hour prior to osimertinib).

Mathematical model of irreversible PK/PD efficacy

Full details of the model are provided in the Supplementary Material. The important aspects of the model, including assumptions, are summarized here. Parent–metabolite pharmacokinetic modeling has been reported extensively in the literature (6). The pharmacokinetics of parent and active metabolite (Fig. 1A) are described by a semiphysiologic compartmental model. The important assumptions are that the parent is cleared solely in the liver and that the fraction converted to metabolite is constant across different routes of dosing.

The pharmacodynamic model (Fig. 1B) represents phosphorylated EGFR (pEGFR), relative to control, as a pool homogenously distributed across the cell and cells in the tumor. Both the parent and active metabolite are considered to bind irreversibly to the ATP-binding pocket of EGFR (4, 5), leading to a reduction in the fraction of pEGFR. The reversible interaction (docking) of the molecule with the receptor is assumed to be more rapid than the covalent binding step and subsequent deactivation of the receptor. The saturable inactivation model describes the reversible kinetics of the molecule entering the ATP-binding pocket (CPU50, CMU50), as well as the consequent covalent bond being formed (K_{bind}; ref. 7). The natural turnover and resynthesis of receptor is represented by K_{rec}, and the rate of drug-induced deactivation is described by K_{bind}

$$\frac{dpEGFR}{dt} = K_{rec}(1 - pEGFR) - pEGFR.K_{bind}\left(\frac{\frac{C_{p,u}}{CPU50} + \frac{C_{m,u}}{CMU50}}{1 + \frac{C_{p,u}}{CPU50} + \frac{C_{m,u}}{CMU50}}\right) \quad (1)$$

On reduction of pEGFR, the rate of cell death is assumed to increase in the tumor and is proportional to pEGFR reduction. The rate of cell death is assumed to be independent of the time pEGFR is reduced; however, the resulting efficacy is integral of the rate of cell death and so, duration of pEGFR will be important for efficacy.

We define f_{kill} where,

$$f_{kill}(pEGFR) = E_{\max} \cdot (1 - pEGFR) \text{ if } n = 1 \quad (2a)$$

and

$$f_{kill}(pEGFR) = E_{\max} \cdot \left(\frac{n^{[1-pEGFR]} - 1}{n - 1}\right) \quad (2b)$$

This relationship captures a "threshold" behavior often observed in biology (see ref. 8 for an example): At small pEGFR perturbations, the system is robust and there is little change in the kill rate. However, when pEGFR is significantly depleted, increased cell death occurs.

Xenograft tumors are assumed to be spherical and composed of a cycling compartment (S_a) near the outside of the tumor (and so near host vasculature) and a noncycling core (C_a; ref. 9). The cycling compartment is assumed to increase in size at a rate proportional (K_{grow}) to the size of the compartment.

$$\frac{dS_a}{dt} = K_{grow}S_a - f_{kill}S_a + J_{Transfer}V_a$$

$$\frac{dC_a}{dt} = -J_{Transfer}V_a$$

To maintain the distance allowed (R_{diff}) of the proliferating compartment from the edge of the tumor, cells are transferred ($J_{Transfer}$) between the proliferating and nonproliferating compartments as the tumor grows or shrinks at a rate proportional to the difference between the current core volume (V_{core}) and the size required for the correctly sized proliferating compartment ($V_{core,Target}$).

$$V_{Core,Target} = \frac{4\Pi}{3}\left(R_{Tumor} - R_{diff}\right)^3$$

$$J_{Transfer} = K_{trans}\left(V_{core} - V_{Core,target}\right)A_{Core}$$

Model parameter estimation

All modeling was carried out in acslXtreme (Aegis Technologies). The residual noise in the pharmacokinetic data was assumed to be proportional to the predicted concentration, whereas for the pharmacodynamic and tumor volume data, it was assumed to be additive. Modeling was carried out in a sequential manner, with pharmacokinetics being analyzed first, then pharmacodynamics with pharmacokinetic parameters fixed, and then finally efficacy.

Results

Estimates of key parameter values are shown in Table 1. All parameter estimates are detailed in Supplementary Table S1.

The pharmacokinetic model describes the combined parent and metabolite pharmacokinetics in the mouse

Pharmacokinetic data from CD-1, SCID, and nude mice were described well by the proposed pharmacokinetic model (Fig. 2). The only variation of parameters across the strains was the fraction absorbed of the parent. The model describes both the kinetics of parent and metabolite together. This demonstrates that the assumptions of linear pharmacokinetics and the conversion of parent to metabolite presystemically and systemically are valid. It should be noted that according to the parameter estimates, a significant fraction (70%) of parent is converted to the active metabolite, resulting in similar exposures of both molecules after oral dosing to mice. Therefore, based upon *in vitro* potency, there will be a significant contribution of the metabolite to the pharmacodynamics and antitumor activity.

ABT alters the clearance of both molecules but not the fraction metabolized to AZ5104

In a separate experiment to investigate the relative potency of parent and metabolite *in vivo*, an irreversible inhibitor of the CYP450 family of drug-metabolizing enzymes ABT was coadministered with osimertinib to modulate the clearance (CL) of both parent and metabolite with the aim of changing the relative systemic concentrations of the two molecules over

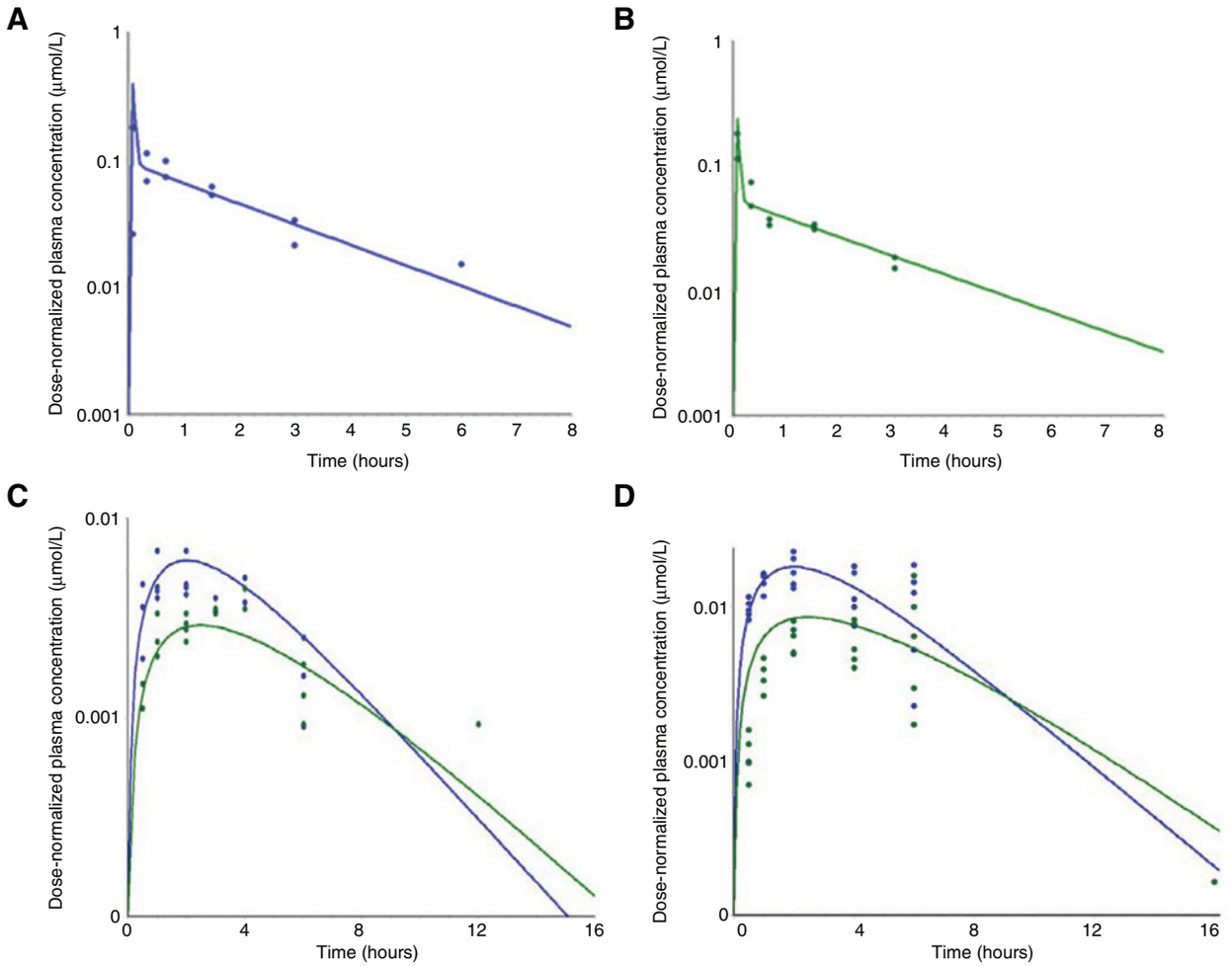

Figure 2.
Data and model of mouse pharmacokinetics across mouse strains. Data (points) and model (solid lines) are shown for parent (blue) and metabolite (green). **A,** parent intravenous (i.v.) CD1. **B,** metabolite intravenous (i.v.) CD1. **C,** nude (oral). **D,** SCID (oral).

time. To understand the effects that ABT had on the pharmacokinetics of osimertinib and AZ5104, each of the model parameters that could potentially change due to changes in metabolism (CL_p, CL_m, fraction metabolized to AZ5104 f_{met}, and fraction absorbed of parent $fabs_p$) were tested to see whether they were significantly different with or without ABT. The result was that only clearance of the two molecules was being altered. From this, it can be deduced that all clearance pathways of the parent were equally inhibited (f_{met} to active metabolite unaltered) and that either there is no gut metabolism or gut metabolism of parent was unchanged ($fabs_p$ unaltered). A comparison of osimertinib and AZ5104 pharmacokinetics with and without ABT is shown in Fig. 3A.

The model can describe the combined pharmacodynamics of osimertinib and AZ5104 as well as the pharmacodynamics of AZ5104 alone

The pharmacodynamic model was then fitted to pEGFR time series data after the administration of osimertinib. Such data were generated in all three xenograft cell lines of interest. The estimated *in vivo* potency of osimertinib and the relative potency of AZ5104 are in reasonable agreement with the *in vitro* values. The correspondence between the *in vitro* and *in vivo* IC_{50}s is likely because of the observation by Schwartz and colleagues (7) that the overall potency of irreversible EGFR inhibitors is largely driven by the reversible binding kinetics.

The model described well the extent and duration of pEGFR reduction relative to control pEGFR (Fig. 4). The active metabolite was also present in all of these experiments, and so while the potency of the parent was recalibrated, the metabolite potency was predicted by fixing the ratio of potencies to the *in vitro* values accounting for differences in protein binding. Note the long duration of effect (>36 hours) in the mutant tumors despite parent and metabolite being virtually eliminated by 16 hours postdose. The pharmacodynamic model captures this by incorporating the irreversible inhibition of available receptor as well as a slow synthesis rate of the new receptor.

To confirm the potency of AZ5104, a second set of pharmacodynamic experiments was carried out *in vivo* in the NCI-H1975 xenograft model. The cytochrome P450 inhibitor ABT was

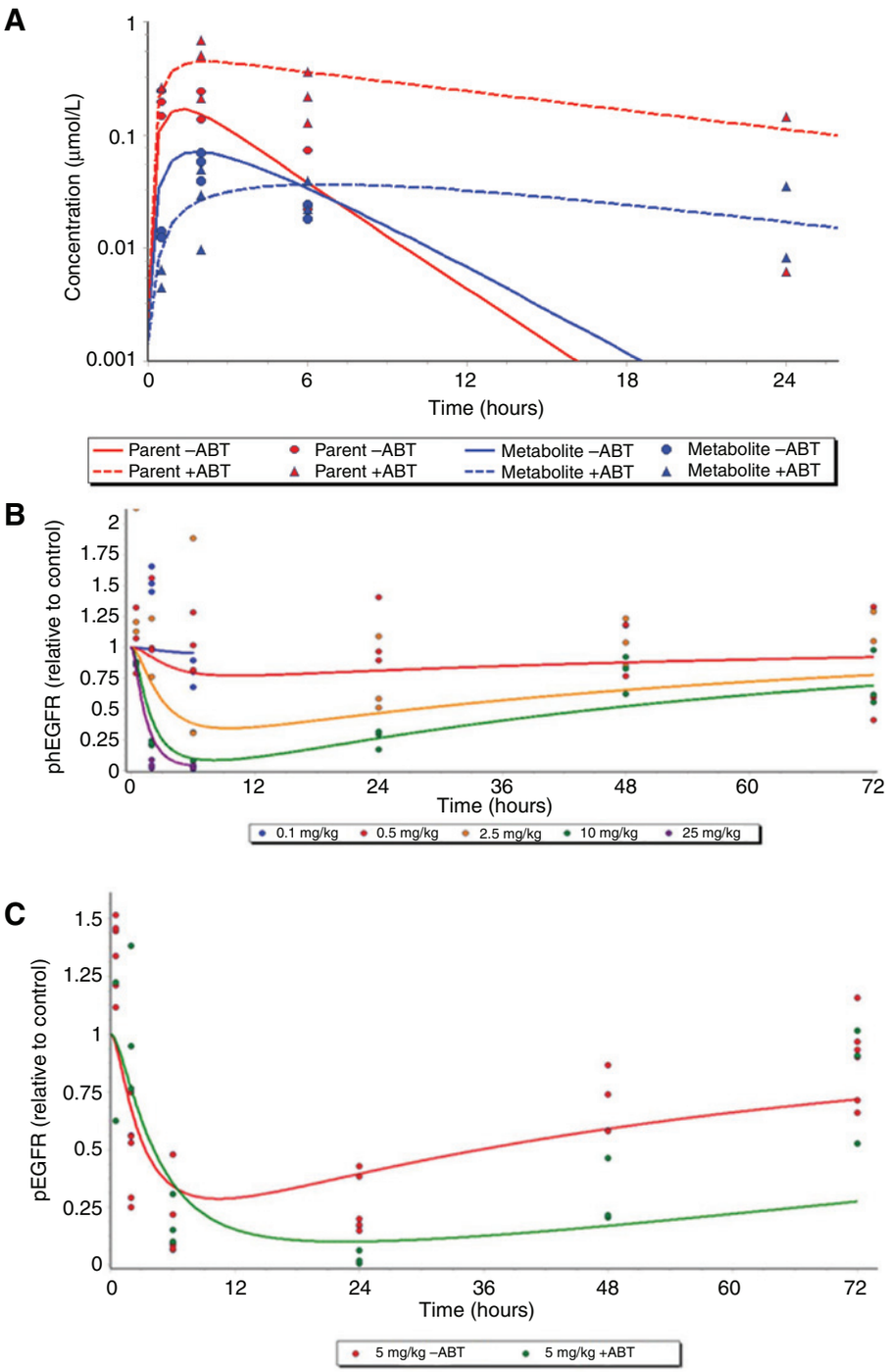

Figure 3.
Investigating the contribution of osimertinib and AZ5104 to the observed pharmacodynamics in the mouse NCI-H1975 xenograft model. **A,** data and model comparing pharmacokinetics of osimertinib and AZ5104 after a 5 mg/kg oral dose of osimertinib with and without codosing ABT. **B,** model and data for pEGFR reduction after administering AZ5104 orally (0.1–25 mg/kg). **C,** coadministering osimertinib (5 mg/kg) with and without ABT.

administered to some of the groups to modulate the pharmacokinetics and so the relative concentrations observed of osimertinib and AZ5104. AZ5104 was also administered orally and demonstrated activity against pEGFR. Simulating the *in vivo*–calibrated PK/PD model, taking into account the effect ABT has on the pharmacokinetics of osimertinib and AZ5104 as well as the direct administration of AZ5104 orally, demonstrated that the fold potency was indeed correct, so the absolute contributions of the two molecules to pharmacodynamic activity have been well characterized (Fig. 3B and C).

Short-term efficacy is described well by the efficacy model simulating repeat dose PK/PD and suggests that pEGFR must be reduced below a threshold value to affect tumor cells

The relationship between efficacy and magnitude and duration of pEGFR reduction was then investigated. There were no repeat

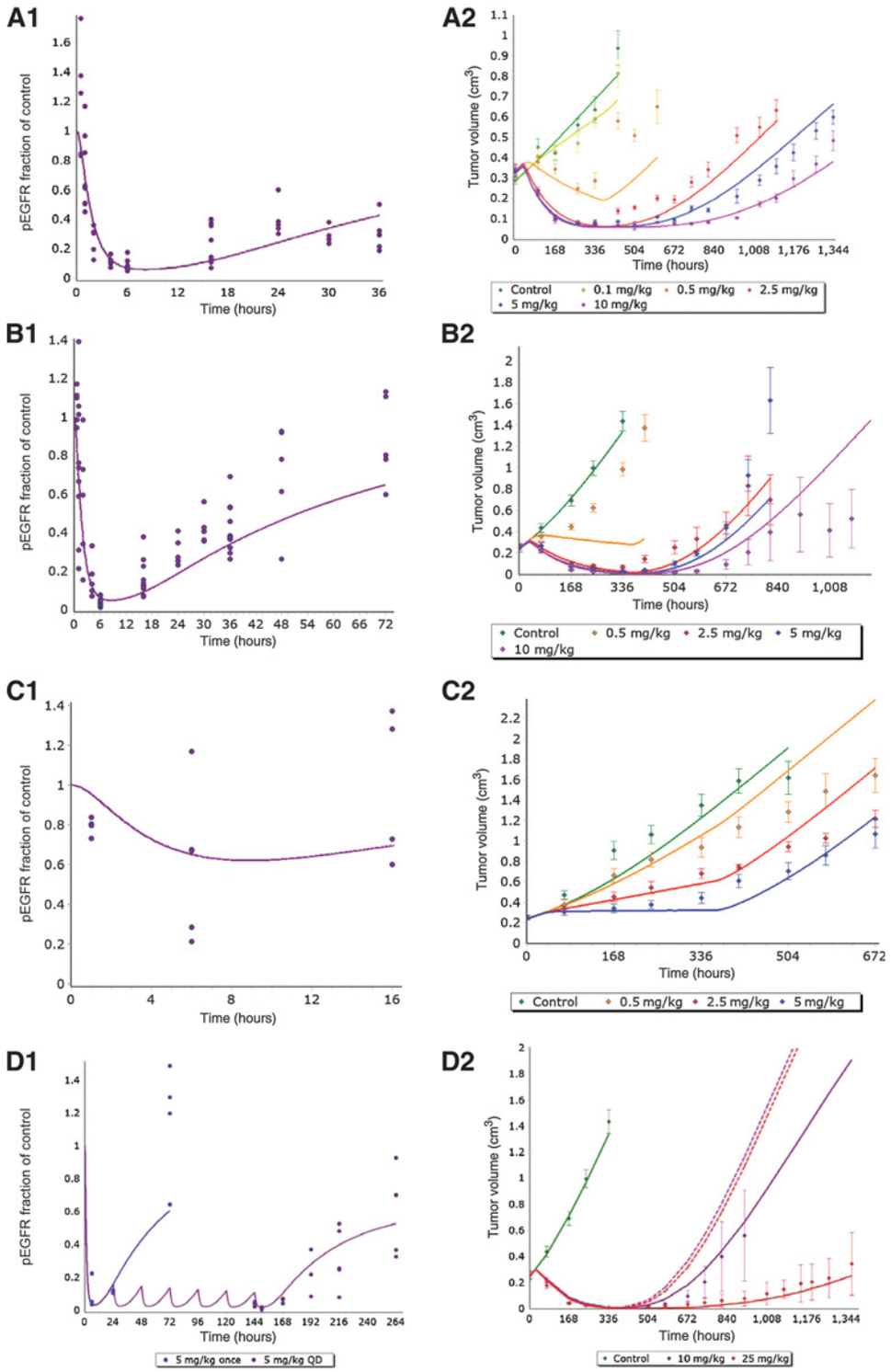

Figure 4.
Model and data for pEGFR reduction after a 5 mg/kg oral dose of osimertinib and tumor volume after oral dosing of osimertinib in the PC9 (**A1** and **A2**), NCI-H1975 (**B1** and **B2**), and A431 (**C1** and **C2**) xenograft models. **D1,** simulation of pharmacodynamic model identified based upon chronic dose efficacy versus observed pEGFR reductions over 7 days of dosing; a simulation of single-dose pharmacodynamics is also shown. QD, daily. **D2,** data and model (modified precursor pool) for chronic dosing efficacy and recovery of tumor growth after dosing ceased. Dashed lines, model prediction without modification to the pEGFR model; solid lines, modified model.

dose PK/PD data available, and so the single dose model developed above was used to simulate repeat dosing assuming this represented the chronic dosing PK/PD relationship. Simulated pEGFR reduction was then linked to an increased death rate in the tumor as described by Eqs. 2a and 2b above. Equations 2a and b describe a relationship that can vary between a graded continuous relationship to one that describes a threshold by modulating the parameter N (Eqs. 2a and 2b). The maximum rate of death E_{max} values were allowed to vary across the three cell lines to characterize differences in sensitivity to pEGFR reduction.

The model could capture the tumor growth curves across a range of once daily doses for 14 days (Fig. 4). The estimates on N across the cell lines (Table 1) were consistent with a threshold relationship, whereby cells are insensitive to moderate reductions in pEGFR. What then differentiates the doses initially is the rate that pEGFR is reduced past this threshold.

Long-term efficacy is not as well described by the PK/PD–TGI model and suggests that a second long-term effect occurs for the receptor

As observed in Fig. 4, pEGFR returns to baseline in about 72 hours following a single oral dose of parent. Given the validated relationship between pEGFR reduction and changes in tumor growth, one would expect when dosing ceases that the tumor should thereafter grow uninhibited. However, tumor growth experiments show that after more than 14 consecutive daily doses, it can then take 2 weeks for the tumor to start growing again.

The explanation used in the mathematical model is that even though pEGFR levels return to baseline within 72 hours following a single dose, it takes 2 weeks to return to baseline following 14 consecutive daily doses. This behavior can be captured mathematically by assuming a pool preceding the turnover model of Fig. 1B that controls the pEGFR receptor synthesis rate (K_{rec}). To explain efficacy, this pool must be relatively insensitive to drug and so is not significantly affected by a single dose. It is however depleted following 14 consecutive doses and is replenished at a very slow rate. As this is now the rate-limiting step, it also dictates the return to baseline of pEGFR, and the slower pEGFR recovery delays the time for tumor regrowth. The pharmacodynamic model (2) was thus modified:

$$\frac{dPOOL}{dt} = K_{pool}\left(1 - POOL\left(1 + KB_{pool}Cp\right)\right) \quad (3)$$

$$\frac{dpEGFR}{dt} = K_{rec}(POOL - pEGFR) - pEGFR.K_{bind}\left(\frac{\frac{C_{p,u}}{CPU50} + \frac{C_{m,u}}{CMU50}}{1 + \frac{C_{p,u}}{CPU50} + \frac{C_{m,u}}{CMU50}}\right) \quad (4)$$

With this modification, the model can adequately capture the slower recovery of tumors. A comparison of the model prediction of tumor volume with and without the precursor pool modification is shown in Fig. 4 D2.

Repeat dose pharmacodynamics inferred from efficacy data confirmed

To test the long-term pEGFR pool hypothesis, a repeat dose PK/PD study was carried out. Osimertinib was dosed once daily for 7 days, and pEGFR was determined at time points on days 1 and 8. The pharmacodynamic model (Eqs. 3 and 4) with the pool component identified from chronic dosing, and washout efficacy was simulated versus the resulting data (Fig. 4 D1). It can be seen that the model predicts well the delayed return to baseline after 7 days dosing in comparison with the return to baseline after a single dose.

Model predicts efficacy for intermittent dosing of osimertinib

Given that osimertinib and AZ5104 are irreversible inhibitors of pEGFR, it was tested whether intermittent dosing of osimertinib in the mouse would result in continued tumor growth suppression. This was found to be the case (Fig. 5A) and further that the model successfully predicted the efficacy resulting without further calibration. The model was then interrogated as to what dose once or twice a week would be required to deliver efficacy equivalent to 5 mg/kg daily (Fig. 5B and C). Based upon simulations of the model, it was concluded that 400 mg/kg once weekly or 100 mg/kg twice weekly would be required. These doses were not tolerated in the mouse and so, 70 mg/kg once and twice weekly were tested. For twice weekly dosing (Fig. 5D), 70 mg/kg osimertinib indeed delivered efficacy similar to 5 mg/kg daily (100 mg/kg predicted). In the case of once weekly dosing, 70 mg/kg (Fig. 5D) resulted in stasis, similar to the prediction of 50 to 100 mg/kg once weekly according to simulations (Fig. 5B). It was concluded that the activity on intermittent dosing could be fully predicted by the intermittent PK/PD simulated by the model and therefore provides evidence that the model can predict antitumor activity when different exposure profiles are delivered. Thus, the model is adequate for further interrogation for simulated human pharmacokinetics. Notably, significantly more drug per week is required for intermittent dosing. This is because although the binding to EGFR is irreversible, the duration of pharmacodynamics as described by the model is dependent upon EGFR protein synthesis. The parameter values reported for the turnover of the receptor, *Krec*, correspond to a pharmacodynamic half-life of around 27 hours. Thus, with the short pharmacokinetic half-life of osimertinib in the mouse, dosing needs to be daily to maintain pEGFR reduction.

Discussion

Linking pharmacokinetics, pharmacodynamics, and disease modification (antitumor activity) for preclinical data allows an insight into how target engagement over time results in changes in tumor growth. This allows the exploration of the consequences of alternative schedules of dosing (perhaps to improve the therapeutic index) as well as how species differences in pharmacokinetics might impact efficacy and therapeutic index. Understanding a quantitative link between target inhibition and efficacy also provides the opportunity to set rational proof-of-mechanism criteria before entering the clinic (3).

Mouse and human pharmacokinetics can be very different, especially in the case considered here, where there was also an active metabolite to consider. This can make dose setting based upon usual considerations, such as C_{max} or AUC questionable. The difficulty is that parent and metabolite are responsible for pharmacodynamics and antitumor activity as well as safety. Mathematical modeling of the time course allows all of this to be integrated. Mouse pharmacokinetics was also modulated using ABT to alter the relative concentrations of parent and metabolite. This provided further insight into *in vivo* pharmacokinetics and validation of the model assumptions.

The irreversible pharmacology of an EGFR inhibitor and its active metabolite has been captured using a modular systems pharmacology approach. We have investigated and accurately described the short- and long-term pharmacodynamic and disease-modifying effects of an irreversible EGFR inhibitor. Furthermore, we have considered intermittent dosing and shown the model can adequately describe the resulting efficacy in the mouse models considered. It is hypothesized that the modeled relationships presented here should be consistent for other irreversible EGFR inhibitors once pharmacokinetics and potency are factored in: The rate of pharmacodynamic response and resulting efficacy is

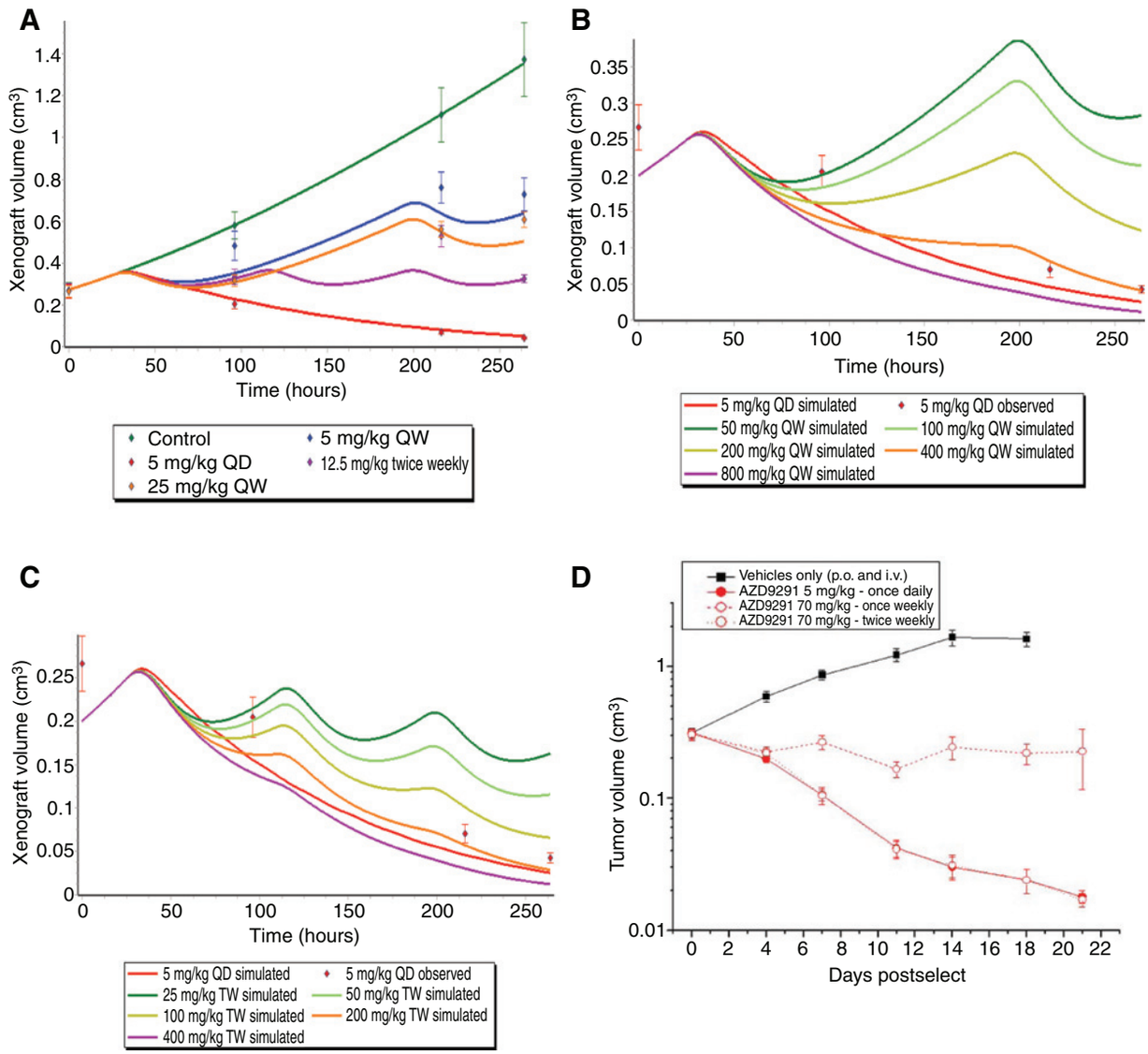

Figure 5.

PK/PD efficacy model in NCI-H1975 predicts intermittent dosing efficacy. **A,** efficacy resulting from low once and twice weekly dosing is predicted by the model without further calibration. QD, daily; QW, once weekly. **B,** simulation of weekly doses of osimertinib in comparison with data from 5 mg/kg daily dose. **C,** simulation of biweekly doses of osimertinib in comparison with data from 5 mg/kg daily dose. TW, twice weekly. **D,** validation of model predictions of intermittent dosing efficacy. p.o., orally; i.v., intravenously.

dependent on biology here, not on a particular small-molecule inhibitor.

Although the modeling presented here is only semimechanistic, it has provided insights through hypothesis generation into the *in vivo* pharmacology of osimertinib, which has allowed the design of targeted confirmatory experiments. Experimental validation has provided confidence in the further use of this model. Primary among the model-based findings was the elucidation of the time-dependent pEGFR pharmacodynamics by noting the disparity between single-dose pharmacodynamics and efficacy. The modeling provided insight into the wild-type EGFR selectivity (compare IC_{50} estimates for A431 vs. PC9 and NCI-H1975 in Table 1) that is important to achieve tolerability of an EGFR inhibitor in the clinic. These results were also valuable in comparing parent and metabolite exposure in patients with that observed in mice at doses causing regressions in tumor xenografts. Given the different pharmacokinetics in human compared with mouse [in human, the half-life was significantly longer, and metabolite concentrations were only about 10% of parent (Supplementary Material; ref. 10)], understanding the potencies of the two molecules was important for the assessment of (i) likely target engagement in the clinic and (ii) expected activity of osimertinib in EGFR T790M mutation-positive NSCLC based upon xenograft model experiments.

Disclosure of Potential Conflicts of Interest

All authors are employees and shareholders of AstraZeneca. No other potential conflicts of interest were disclosed by the authors.

Authors' Contributions

Conception and design: J.W.T. Yates, S. Ashton, D. Cross, P. Ballard
Development of methodology: J.W.T. Yates, S.J. Powell
Acquisition of data (provided animals, acquired and managed patients, provided facilities, etc.): S. Ashton
Analysis and interpretation of data (e.g., statistical analysis, biostatistics, computational analysis): J.W.T. Yates, D. Cross, S.J. Powell, P. Ballard
Writing, review, and/or revision of the manuscript: J.W.T. Yates, S. Ashton, D. Cross, P. Ballard
Administrative, technical, or material support (i.e., reporting or organizing data, constructing databases): S.J. Powell, P. Ballard
Study supervision: S. Ashton, M.J. Mellor

Acknowledgments

The authors thank Richard Dimelow for initial PK/PD model development, Didier Dannilon and Jo Wilson for mouse pharmacokinetics, and Gareth Hughes, Amar Rahi, David Smith, Keith Welsh, Emily Lawrie, Michelle Scott, Jon Orme, and Michael Hulse for *in vitro* and *in vivo* pharmacodynamic and efficacy data. Some studies were run at Oncodesign.

The costs of publication of this article were defrayed in part by the payment of page charges. This article must therefore be hereby marked *advertisement* in accordance with 18 U.S.C. Section 1734 solely to indicate this fact.

Received March 17, 2016; revised July 11, 2016; accepted July 12, 2016; published OnlineFirst July 20, 2016.

References

1. Milligan PA, Brown MJ, Marchant B, Martin SW, van der Graaf PH, Benson N, et al. Model-based drug development: a rational approach to efficiently accelerate drug development. Clin Pharmacol Ther 2013;9:502–14.
2. Visser SAG, Aurell M, Jones RDO, Schuck VJA, Egnell A-C, Peters S, et al. Model-based drug discovery: implementation and impact. Drug Discov Today 2013;18:764–75.
3. Bueters T, Ploeger BA, Visser SAG. The virtue of translational PKPD modelling in drug discovery: selecting the right clinical candidate while sparing animal lives. Drug Discov Today 2013;18:853–62.
4. Finlay MRV, Anderton M, Ashton S, Ballard P, Bethel PA, Box MR, et al. Discovery of a potent and selective EGFR inhibitor (AZD9291) of both sensitizing and T790M resistance mutations that spares the wild type form of the receptor. J Med Chem 2014;57:8249–67.
5. Cross DAE, Ashton SE, Ghiorghiu S, Eberlein C, Nebhan CA, Spitzler PJ, et al. AZD9291, an irreversible EGFR TKI, overcomes T790M-mediated resistance to EGFR inhibitors in lung cancer. Cancer Discov 2014;4:1046–61.
6. Cheung SYA, Yates JWT, Aarons L. The design and analysis of parallel experiments to produce structurally identifiable models. J Pharmacokinet Pharmacodyn 2013;40:93–100.
7. Schwartz PA, Kuzmic P, Solowiej J, Bergqvist S, Bolanos B, Almaden C, et al. Covalent EGFR inhibitor analysis reveals importance of reversible interactions to potency and mechanism of drug resistance. Proc Natl Acad Sci U S A 2014;111:173–8.
8. Kirouac DC, Du JY, Lahdenranta J, Overland R, Yarar D, Paragas V, et al. Computational modeling of ERBB2-amplified breast cancer identifies combined ErbB2/3 blockade as superior to combination of MEK and AKT inhibitors. Sci Signal 2013;6:ra68.
9. Evans ND, Dimelow RJ, Yates JWT. Modelling of tumor growth and cytotoxic effect of docetaxel in xenografts. Comput Methods Programs Biomed 2014;114:e3–e13.
10. Jänne PS, Yang JC-H, Kim D-W, Planchard D, Ohe Y, Ramalingham SS, et al. AZD9291 in EGFR inhibitor-resistant non-small-cell lung cancer. N Engl J Med 2015;372:1689–99.